

**Manuscript version: Author's Accepted Manuscript**

The version presented in WRAP is the author's accepted manuscript and may differ from the published version or Version of Record.

**Persistent WRAP URL:**

<http://wrap.warwick.ac.uk/149340>

**How to cite:**

Please refer to published version for the most recent bibliographic citation information. If a published version is known of, the repository item page linked to above, will contain details on accessing it.

**Copyright and reuse:**

The Warwick Research Archive Portal (WRAP) makes this work by researchers of the University of Warwick available open access under the following conditions.

© 2020 Elsevier. Licensed under the Creative Commons Attribution-NonCommercial-NoDerivatives 4.0 International <http://creativecommons.org/licenses/by-nc-nd/4.0/>.



**Publisher's statement:**

Please refer to the repository item page, publisher's statement section, for further information.

For more information, please contact the WRAP Team at: [wrap@warwick.ac.uk](mailto:wrap@warwick.ac.uk).

# **Solution of the ultimate bearing capacity at the tip of a pile in inclined rocks based on the Hoek-Brown criterion**

Yuanqiang Cai<sup>a, b</sup>, Bin Xu<sup>a</sup>, Zhigang Cao<sup>a, \*</sup>, Xueyu Geng<sup>c</sup>, Zonghao Yuan<sup>b</sup>

<sup>a</sup>College of Civil Engineering and Architecture, Zhejiang University, Hangzhou 310058, PR China

<sup>b</sup>College of Civil Engineering and Architecture, Zhejiang University of Technology, Hangzhou 310014, PR China

<sup>c</sup>School of Engineering (F332), The University of Warwick, Coventry, CV4 7AL, UK

**Abstract:** To investigate the bearing mechanism of piles in inclined slope, this paper proposed an analytical method through geometric transformation to calculate the ultimate bearing capacity at the tip of a pile in inclined rocks based on the characteristic line method. It was found that there were five failure modes for piles in inclined rocks depending on the embedment ratios, slope angles, average overburden load and tensile strength parameter of the rock mass. When the pile failure mode was under the modes of deep pile with minor overburden (DL) and deep pile with major overburden (DH), the ultimate bearing capacity had no change as the slope angle and the pile embedment ratio changed. When the pile was under the failure modes of semi-deep pile with minor overburden (SL), semi-deep pile with major overburden (SH) or shallow pile (SS), the ultimate bearing capacity decreased with an increasing rate as the slope angles increased; and to get the same ultimate bearing capacity at the pile tip, the pile embedment ratio should increase. The proposed analytical method can be served as an efficient method to estimate the bearing capacity of piles in inclined slope with small slope angle (typically less than 40°).

**Key words:** Pile on inclined rock; bearing capacity; slope angles; embedment ratio

## **1. Introduction**

With the rapid development of transportation facilities and electric power grids in China, more and more pile foundations are built in high and steep slopes in mountain area. The topography, landforms and geological conditions in these areas are very complicated and the steep slopes are usually covered with thin or no soil layers, thus many of the piles on the slope are rock-socketed piles.

For shallow foundations in flat soils or rocks, bearing capacity of foundations was a classic problem and had been investigated mainly through the limit equilibrium

method, the slip method and the limit analysis method. Terzaghi [1] presented a theoretical solution for calculating the ultimate bearing capacity of shallow foundations at different depths and site conditions. Hansen [2] considered the compressibility of soil and suggested a comparison between the stiffness index and the critical stiffness index of the soil, to discriminate the mode of soil failure. Meyerhof [3] proposed the ultimate bearing capacity formula considering the influence of shear strength on the soil. Based on the limit equilibrium theory of loose media, Sokolovskii [4] employed the characteristic line numerical solution to obtain the ultimate bearing capacity of foundation under the certain boundary conditions. Later, Serrano and Olalla [5-9] considered the ultimate bearing capacity of foundations on rock masses based on the Hoek-Brown failure criterion and modified Hoek-Brown failure criterion. Yang [10,11] had focused on the ultimate bearing capacity of a strip footing with the modified failure criterion using the technique, an MC linear failure criterion, was proposed to calculate the rate of external work and internal energy dissipation.

For shallow foundations near the inclined slope of soils or rocks, Serrano and Olalla [12,13] analyzed the strip load on a homogeneous, isotropic and continuous mass with a modified Mohr-Coulomb failure criterion using the method of characteristics lines. Cheng [14,15] firstly demonstrated the equivalence between the classical lateral earth pressure and bearing capacity problem by the slip line method. Based on these results, it was concluded that the three classical problems were equivalent in the basic principles, and each problem can be viewed as the inverse of the other problems.

On the basis of plasticity, Meyerhof [3] had developed the bearing capacity theory by extending the previous surface foundation bearing capacity formula to shallow foundations and deep foundations. For piles in flat rock, Serrano and Olalla [16,17] proposed a method for calculating the ultimate bearing capacity at the tip of a pile embedded in flat rock, expanding and applying Meyerhof's theory. However, these studies focused on the solution of the ultimate bearing capacity at the tip of piles in flat ground. In the engineering practice, piles were constructed in the inclined rocks under many occasions. The bearing mechanism of the pile in the inclined rocks remains unclear, thus it is necessary to investigate the bearing capacity of piles in inclined rocks to know the bearing mechanism deeply and supply design guidelines for the piles.

Based on the characteristic line method, this paper proposed an analytical method to calculate the ultimate bearing capacity at the tip of a pile in inclined rocks with different slope angles. Different failure modes for piles were identified under different embedment ratios and slope angles. The effects of slope angles and embedment ratios on the pile bearing capacity was specially investigated under different failure modes.

## 2. Basic hypotheses and failure criterion

Fig.1 shows the sketch of assumed failure surface of the pile. The rock mass is assumed to be a homogeneous, isotropic and continuous mass medium. The ultimate bearing capacity at the tip of piles in inclined rocks was calculated based on Hoek-Brown strength criterion [18]. The rock medium fails mainly when the failure zone is obtained using the characteristic lines method.. The rock mass is weightless and it is assumed that the material is coaxial and has associated dilatancy [16,17].

The Hoek-Brown criterion [16,17] is given as follows:

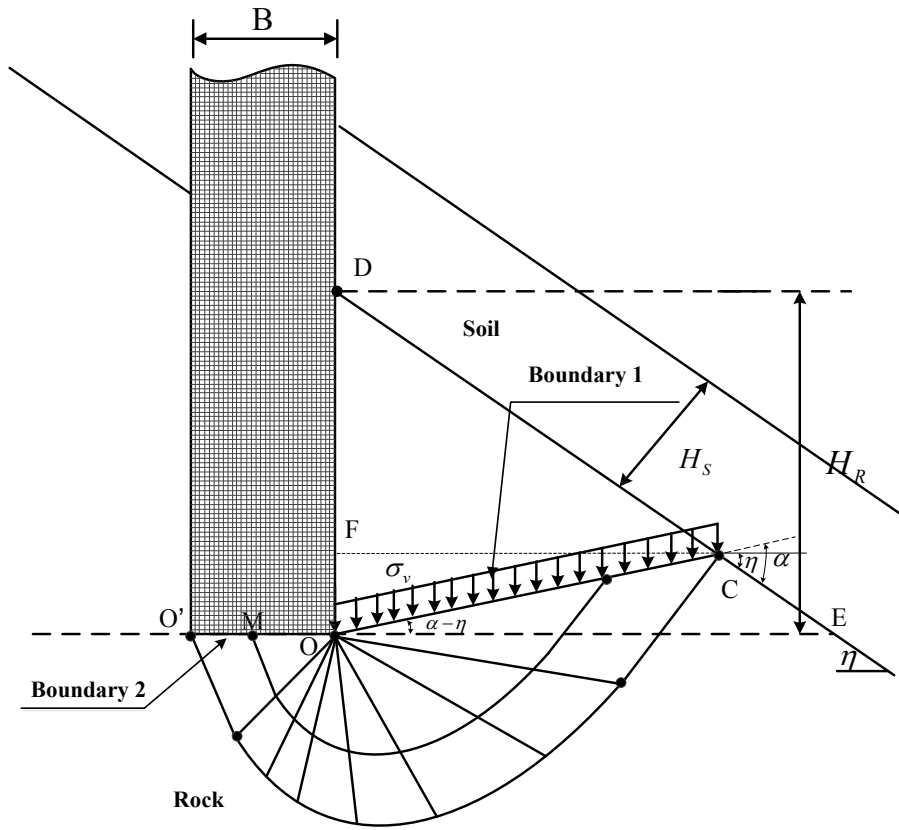
$$\frac{\sigma_I^* - \sigma_{III}^*}{\sigma_c} = \sqrt{m \frac{\sigma_{III}^*}{\sigma_c} + s} \quad (2.1)$$

where  $\sigma_I^*$  is the major failure stress and  $\sigma_{III}^*$  is the minor failure stress,  $\sigma_c$  is the unconfined compressive strength,  $m$  and  $s$  are Hoek-Brown constants.

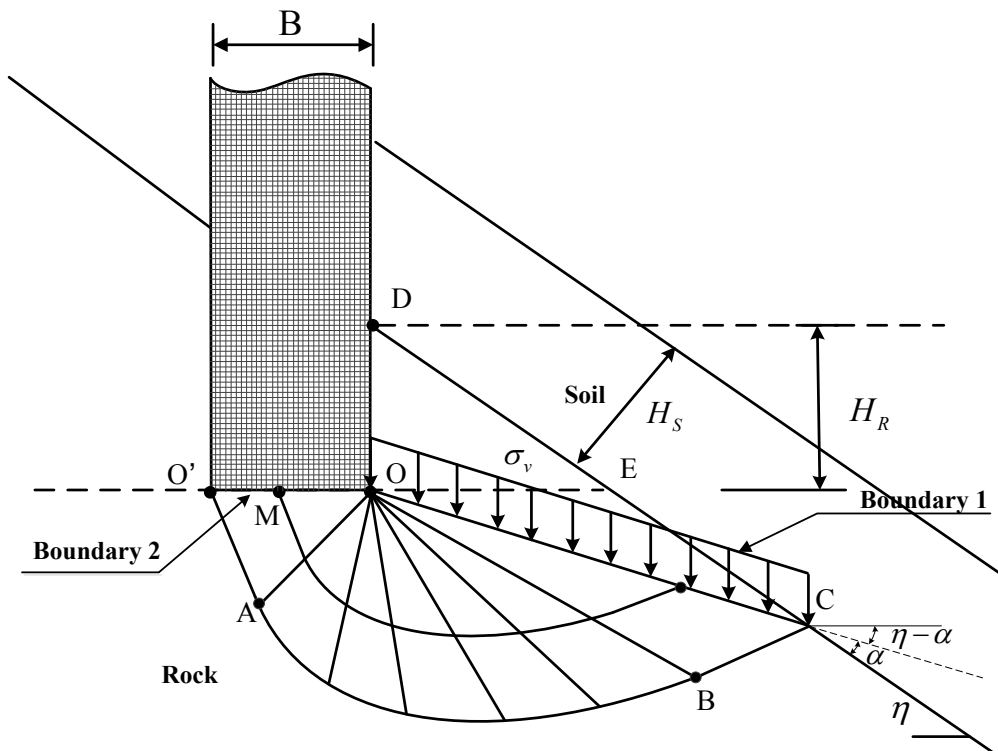
The slope angle  $\eta$  and the virtual angle  $\alpha$  are known (Fig.1). The embedment ratio  $n$  is defined as:

$$n = \frac{H_R}{B} = \frac{DO}{OO'} \quad (2.2)$$

The instantaneous friction angles  $\rho_1$  and  $\rho_2$  for Boundaries 1 and 2, respectively.



(a)  $\alpha > \eta$



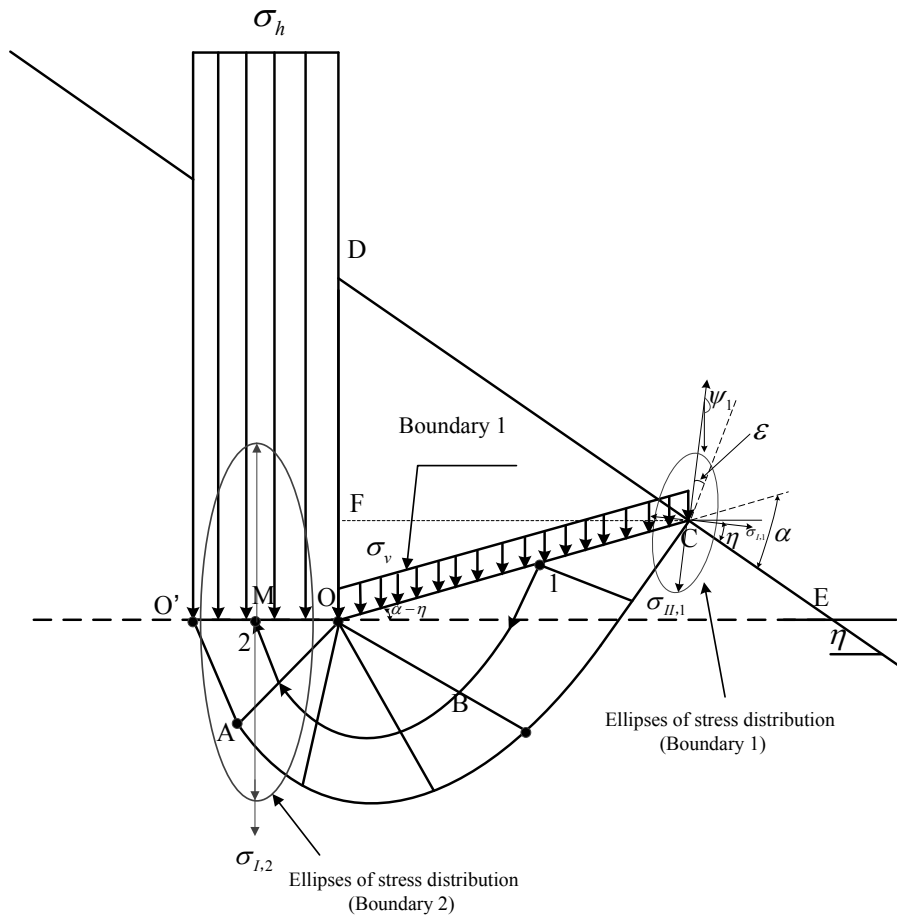
(b)  $\alpha \leq \eta$

Fig.1. Sketch of assumed failure

Fig.2 mainly shows the ultimate bearing capacity  $\sigma_h$  and a load  $\sigma_v$  for Boundary 1.

$\sigma_h$ —ultimate bearing capacity under two-dimensionality hypothesis (kN/m<sup>2</sup>).

$\sigma_v$ — vertical load exerted on Boundary 1.



(a)  $\alpha > \eta$

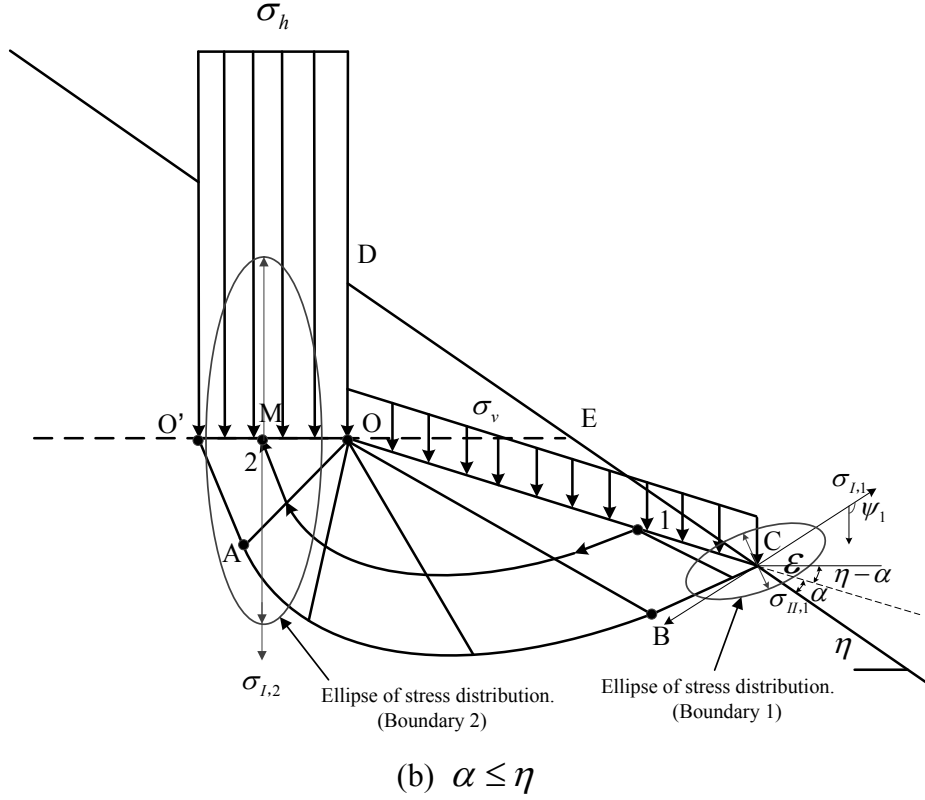


Fig.2. Force diagram and stress ellipses.

When  $\alpha > \eta$ , the normal components ( $\sigma$ ) and shear components ( $\tau$ ) are as follows:

$$\begin{cases} s_1 = \sigma_v \cos(\alpha - \eta) = h_m \cos^2(\alpha - \eta) \\ \tau_1 = \sigma_v \sin(\alpha - \eta) = h_m \sin(\alpha - \eta) \cos(\alpha - \eta) \end{cases} \quad (2.3)$$

When  $\alpha \leq \eta$ , the normal ( $\sigma$ ) and shear ( $\tau$ ) components are as follows:

$$\begin{cases} s_1 = \sigma_v \cos(\eta - \alpha) = h_m \cos^2(\eta - \alpha) \\ \tau_1 = \sigma_v \sin(\eta - \alpha) = h_m \sin(\eta - \alpha) \cos(\eta - \alpha) \end{cases} \quad (2.4)$$

$h_m$  — average overburden load in ground.

Taking into account formula (2.3) and (2.4), the angle for virtual boundary 1 is expressed as:

$$\begin{cases} \cos^2(\alpha - \eta) = \frac{(p_1)^2 - (q_1)^2}{2p_1 h_m - h_m^2} (\alpha > \eta) \\ \cos^2(\eta - \alpha) = \frac{(p_1)^2 - (q_1)^2}{2p_1 h_m - h_m^2} (\alpha \leq \eta) \end{cases} \quad (2.5)$$

### 3. The solution procedure

When  $\alpha > \eta$ , the embedment ratio  $n$  is (Fig.1):

$$\begin{aligned} n &= \frac{H_R}{B} = \frac{OC * \sin(\alpha - \eta) + DC * \sin \eta}{2OM} \\ &= \frac{\sin(\alpha - \eta)}{2} * \frac{OC}{OM} + \frac{\sin \eta}{2} * \frac{DC}{OM} \end{aligned} \quad (3.1)$$

$$\begin{aligned} n &= \frac{\sin(\alpha - \eta)}{2} * \left(\frac{OC}{OB}\right) * \left(\frac{OB}{OA}\right) * \left(\frac{OA}{OM}\right) \\ &+ \frac{\sin \eta}{2} * \left(\frac{DC}{FC}\right) * \left(\frac{FC}{OC}\right) * \left(\frac{OC}{OB}\right) * \left(\frac{OB}{OA}\right) * \left(\frac{OA}{OM}\right) \end{aligned} \quad (3.2)$$

When  $\alpha \leq \eta$ , the embedment ratio  $n$  is (Fig.1):

$$n = \frac{H_R}{B} = \frac{OC * \sin \alpha}{2OM * \cos \eta} = \frac{\sin \alpha}{2 \cos \eta} * \frac{OC}{OM} \quad (3.3)$$

$$n = \frac{\sin \alpha}{2 \cos \eta} * \left(\frac{OC}{OB}\right) * \left(\frac{OB}{OA}\right) * \left(\frac{OA}{OM}\right) \quad (3.4)$$

According to Serrano and Olalla [7]:

$$\frac{OC}{OB} = \frac{\sin 2u_1}{\sin(u_1 + \varepsilon)} = \frac{2 \sin u_1 \cos u_1}{\sin(u_1 + \varepsilon)} \quad (3.5)$$

$$\frac{OB}{OA} = \frac{\sqrt{\tan \rho_1} \sqrt{1 - \sin \rho_2}}{\sqrt{\tan \rho_2} \sqrt{1 - \sin \rho_1}} = \frac{\sqrt{\tan \rho_1} \sin u_2}{\sqrt{\tan \rho_2} \sin u_1} \quad (3.6)$$

$$\frac{OA}{OM} = \frac{1}{\sin u_2} \quad (3.7)$$

After some manipulations, the following equation holds:

$$n = \begin{cases} \left[ \sin(\alpha - \eta) + \tan \eta \cos(\alpha - \eta) \right] \frac{\cos\left(\frac{\pi - \rho_1}{4} - \frac{\rho_1}{2}\right)}{\sin\left[\left(\frac{\pi - \rho_1}{4} - \frac{\rho_1}{2}\right) + \varepsilon\right]} \sqrt{\frac{\tan \rho_1}{\tan \rho_2}} & (\alpha > \eta) \\ \frac{\sin \alpha}{\cos \eta} \frac{\cos\left(\frac{\pi - \rho_1}{4} - \frac{\rho_1}{2}\right)}{\sin\left[\left(\frac{\pi - \rho_1}{4} - \frac{\rho_1}{2}\right) + \varepsilon\right]} \sqrt{\frac{\tan \rho_1}{\tan \rho_2}} & (\alpha \leq \eta) \end{cases} \quad (3.8)$$

This equation expresses the embedment ratio  $n$  against the angle  $\alpha$  and  $\eta$ .

When minor overburden circle  $h_m < 2\sqrt{2\zeta}$ , the limiting embedment condition

$n_{L2}^S$  is reached, which is expressed as:

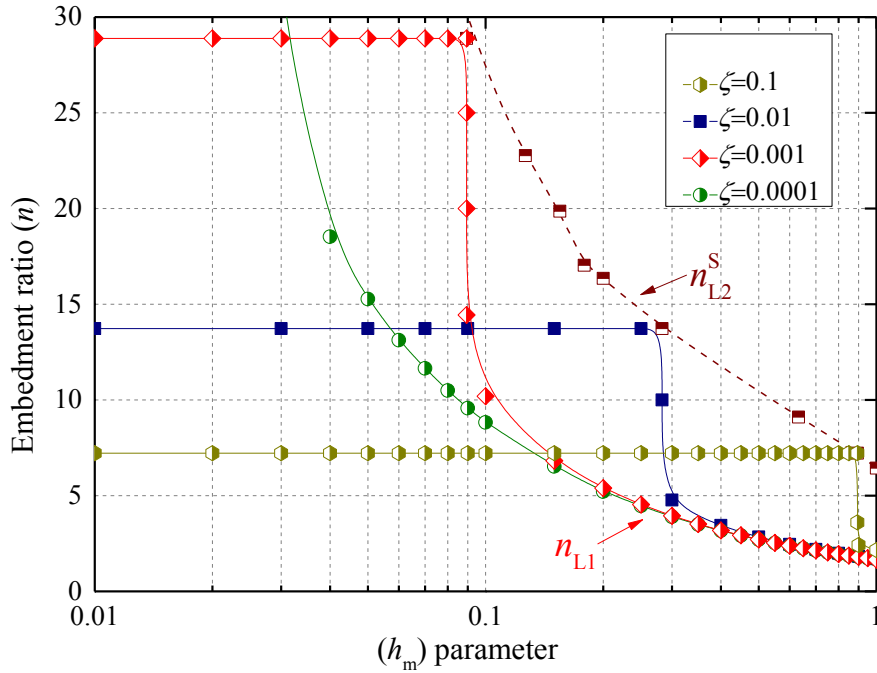


$$n_{L2}^S = \cot\left(\frac{\pi}{4} - \frac{\rho_1}{2}\right) \sqrt{\frac{\tan \rho_1}{\tan \rho_2}} = n_{L2}(\zeta) \quad (3.9)$$

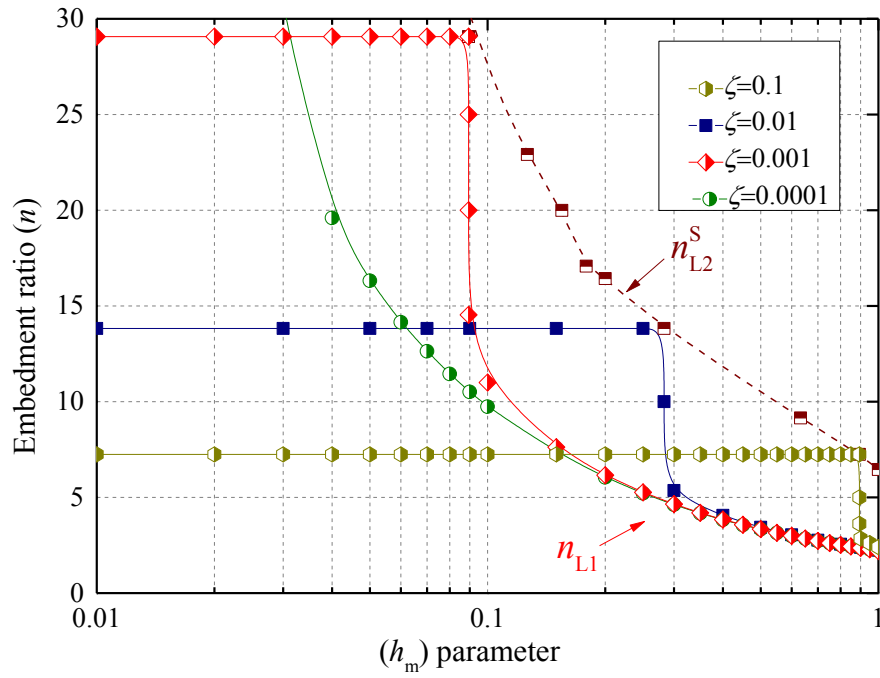
When major overburden circle  $h_m > 2\sqrt{2\zeta}$ , the limiting embedment condition  $n_{L1}$  occurs which can be expressed as following:

$$n_{L1} = [\sin(\alpha_{L1} - \eta) + \tan \eta \cos(\alpha_{L1} - \eta)] \frac{\cos\left(\frac{\pi}{4} - \frac{\rho_{L1}}{2}\right)}{\sin\left[\left(\frac{\pi}{4} - \frac{\rho_{L1}}{2}\right) + \varepsilon_{L1}\right]} \sqrt{\frac{\tan \rho_{L1}}{\tan \rho_2}} = n_{L1}(\zeta, h_m) \quad (3.10)$$

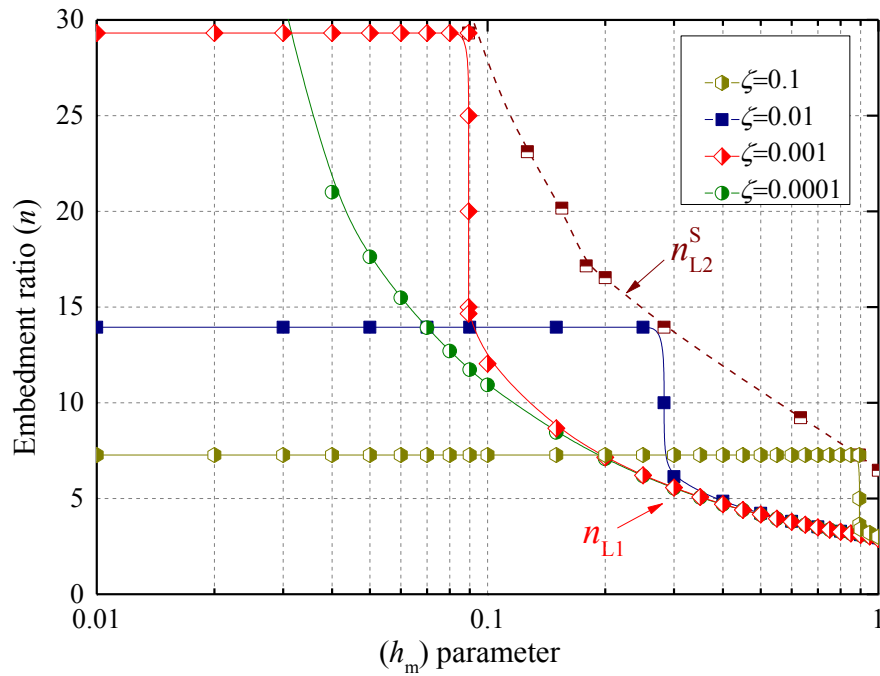
Fig.3 shows the embedment ratio  $n$  against the overburden pressure  $h_m$  for different values of parameter  $\zeta$ . When  $h_m < 2\sqrt{2\zeta}$ , the embedment ratio has no change because it is separated by the limiting embedment  $n_{L2}^S$ . When  $h_m = 2\sqrt{2\zeta}$ , the embedment ratio has the turning point and abruptly decreases. When  $h_m > 2\sqrt{2\zeta}$ , the embedment ratio decreases with the increasing parameter  $h_m$ . The limiting embedment ratio  $n_{L2}^S$  and  $n_{L1}$  decrease as the parameter  $h_m$  increases.



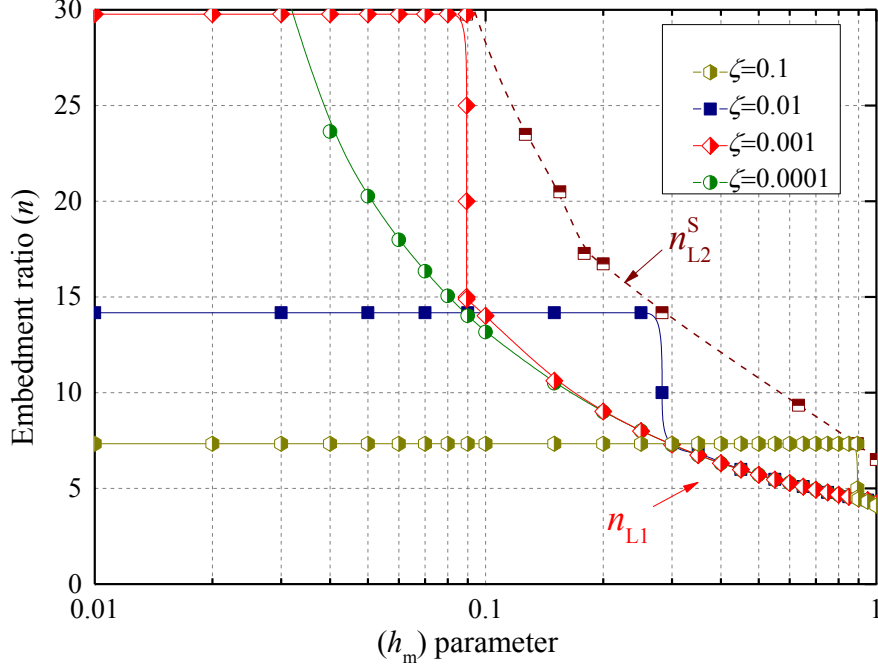
(a)  $\eta=0^\circ$



(b)  $\eta=20^\circ$



(c)  $\eta=40^\circ$



(d)  $\eta=60^\circ$

Fig.3. The relation between the embedment ratio  $n$  and the overburden pressure  $h_m$  for different  $\zeta$ .

For the case of  $\alpha > \eta$ , Fig.4 presents the four pile failure modes which are determined by the overburden  $h_m$  and the embedment ratio  $n$  for different slope angles. When  $h_m < 2\sqrt{2\zeta}$ , the failure mode of the pile were divided by the limiting embedment ratio  $n_{L2}^S$  into two modes: deep foundation piles with a minor overburden (DL) for  $n > n_{L2}^S$  and semi-deep foundation piles with a minor overburden (SL) for  $n < n_{L2}^S$ . When  $h_m > 2\sqrt{2\zeta}$ , the failure mode of the pile were divided by the limiting embedment ratio  $n_{L1}$  into the modes of deep foundation piles with a major overburden (DH) for  $n > n_{L1}$  and semi-deep foundation piles with a major overburden (SH) for  $n < n_{L1}$ .

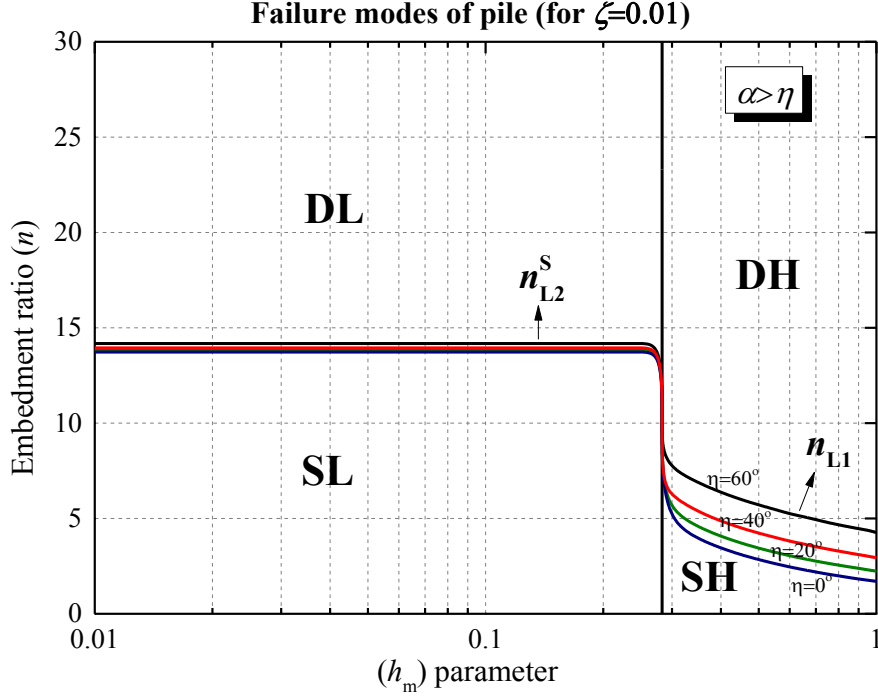


Fig.4. Failures modes of pile under the different slope angles  $\eta$  ( $\alpha > \eta$ ).

Fig.5 shows the variation of the limiting embedment ratio with the change of  $\eta$ .

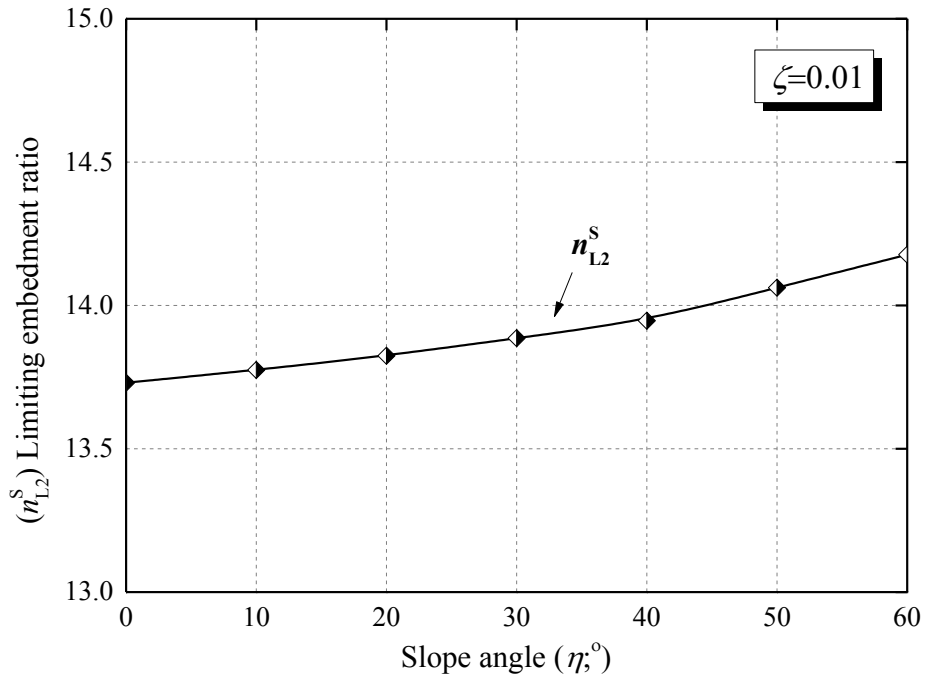
When  $h_m < 2\sqrt{2\zeta}$ , the limiting embedment condition  $n_{L2}^S$  is expressed as:

$$n_{L2}^S = \cot\left(\frac{\pi}{4} - \frac{\rho_1}{2}\right) \sqrt{\frac{\tan \rho_1}{\tan \rho_2}} \quad (3.11)$$

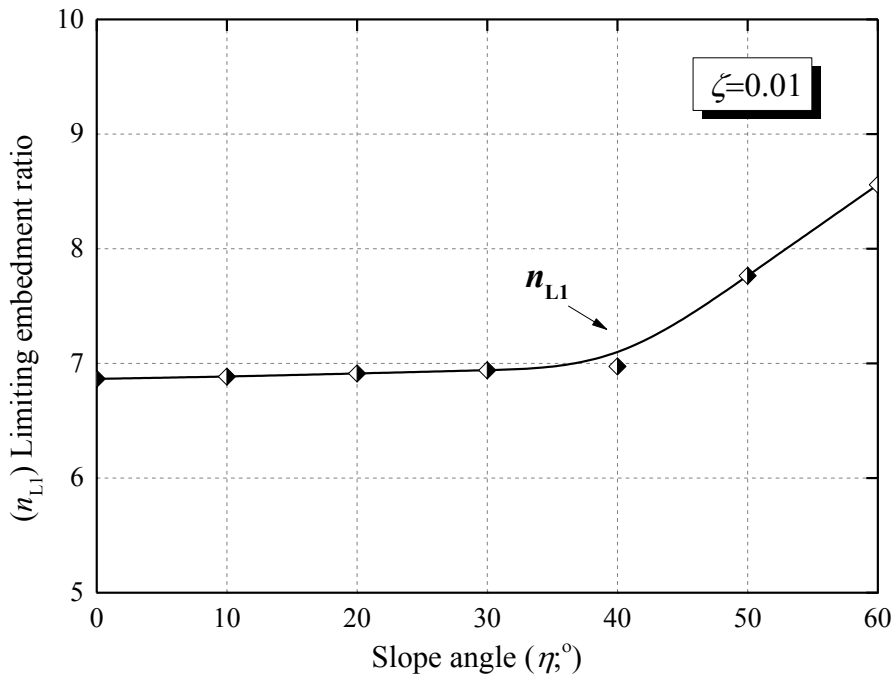
As shown in Fig.5 (a), the limiting embedment ratio  $n_{L2}^S$  increases with increasing slope angles. While for the case of  $h_m > 2\sqrt{2\zeta}$  shown in Fig.5 (b), the limiting embedment condition  $n_{L1}$  is expressed as:

$$n_{L1} = \left[ \sin(\alpha_{L1} - \eta) + \tan \eta \cos(\alpha_{L1} - \eta) \right] \frac{\cos\left(\frac{\pi}{4} - \frac{\rho_{L1}}{2}\right)}{\sin\left[\left(\frac{\pi}{4} - \frac{\rho_{L1}}{2}\right) + \varepsilon_{L1}\right]} \sqrt{\frac{\tan \rho_{L1}}{\tan \rho_2}} \quad (3.12)$$

The limiting embedment ratio  $n_{L1}$  keeps almost constant when  $\eta \leq 40^\circ$  and increases rapidly as the slope angle  $\eta$  increases further.



(a). The relation between the limiting embedment ratio  $n_{L2}^S$  and different slope angles  $\eta$ .



(b). The relation between the limiting embedment ratio  $n_{L1}$  and different slope angles  $\eta$ .

Fig.5. The variation of the limiting embedment ratio with the change of slope angles  
 For the case of  $\alpha \leq \eta$ , it is under the failure mode of shallow foundation piles (SS). Fig.6 shows the variation in the embedment ratio  $n$  with different overburden

pressures  $h_m$ . The embedment ratio has no turning point of overburden pressure load and the embedment ratio decreases with increasing slope angles.

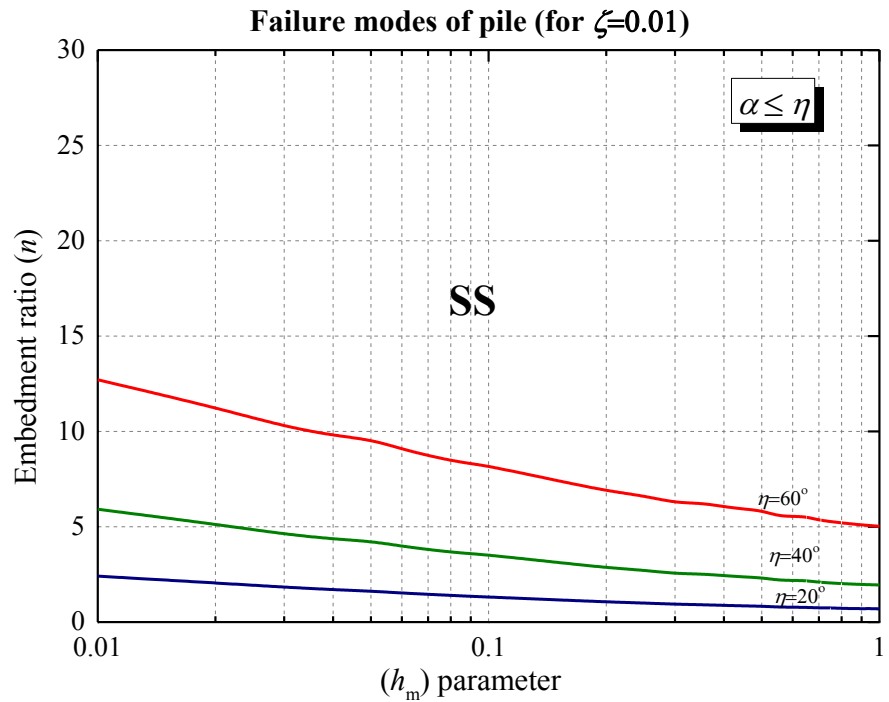
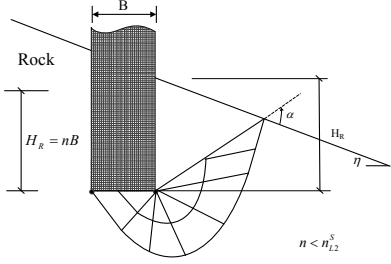
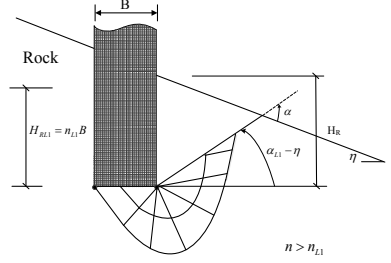
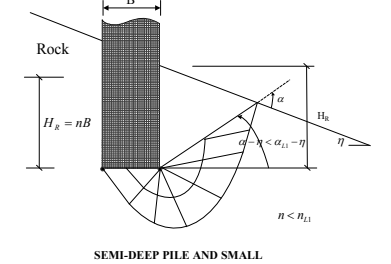
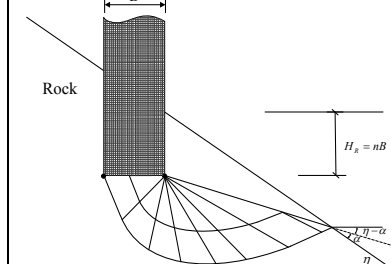


Fig.6. Failures modes of pile under the different slope angles  $\eta$  ( $\alpha \leq \eta$ ).

Based on the analysis above, the five failure modes of the piles in inclined rock under different conditions are summarized in Table.1.

Table. 1 Failure modes of piles in inclined rock

	Average overburden load in ground	Embedment ratio	Failure modes of pile	
		$n > n_{L2}^S$	Deep pile and small overburden (DL)	<p style="text-align: center;">DEEP PILE AND SMALL OVERBURDEN (DL)</p>

$\alpha > \eta$	$h_m < 2\sqrt{2\zeta}$	$n < n_{L2}^S$	Semi-deep pile and small overburden (SL)	 <p style="text-align: center;">SEMI-DEEP PILE AND SMALL OVERBURDEN (SL)</p>
	$h_m > 2\sqrt{2\zeta}$	$n > n_{L1}$	Deep pile and large overburden (DH)	 <p style="text-align: center;">DEEP PILE AND SMALL OVERBURDEN (DH)</p>
		$n < n_{L1}$	Semi-deep pile and large overburden (SH)	 <p style="text-align: center;">SEMI-DEEP PILE AND SMALL OVERBURDEN (SH)</p>
$\alpha \leq \eta$			Shallow pile (SS)	 <p style="text-align: center;">SHALLOW PILE (SS)</p>

#### 4. Ultimate bearing capacity of a pile tip

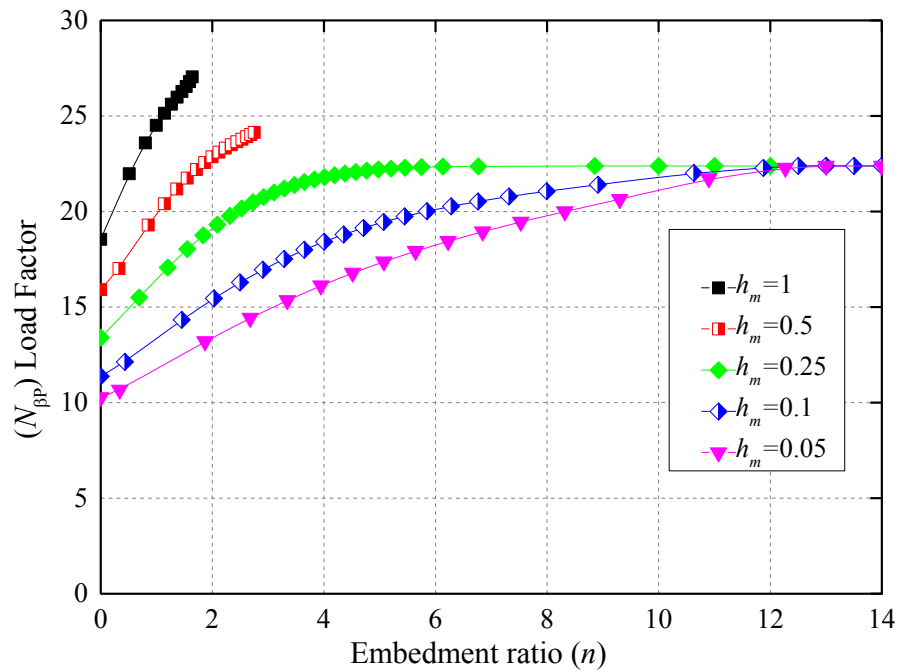
The ultimate bearing capacity at the tip of a pile ( $\sigma_{hp}^*$ ) is

$$\sigma_{hp}^* = \beta(N_\beta - \zeta)s_\beta = \beta N_{\beta P} \quad (4.1)$$

$s_\beta$  — shape coefficient.

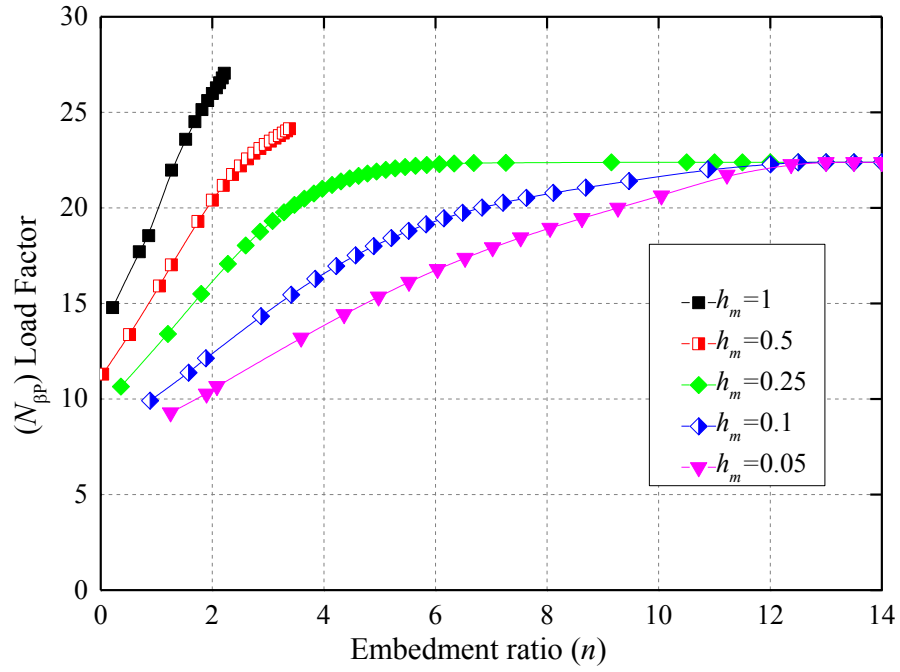
Fig.7 shows the load factor  $N_{\beta P}$  against the embedment ratio  $n$ , for different overburdens  $h_m$  and different angles  $\eta$ . When  $h_m < 2\sqrt{2\zeta}$  ( $h_m=0.25, 0.1$  and

0.05), the load factor increases dramatically then tends to reach a constant value after  $n$  reaches or exceeds the limit embedment ratios  $n_{L2}^S$ , and the pile failure mode transits from SL to DL. When  $h_m > 2\sqrt{2\zeta}$  ( $h_m=0.5$  and  $1.0$ ), the load factor increases dramatically then end abruptly when intersected by the limit embedment ratios  $n_{L1}$  and the pile is under the failure mode of SH and will transit to DH failure mode, as the embedment ratios increases further. Comparison between Figs.7 (a)-(d) reveals that the limit depth  $n_{L1}$  and  $n_{L2}^S$  increases with increasing slope angles.

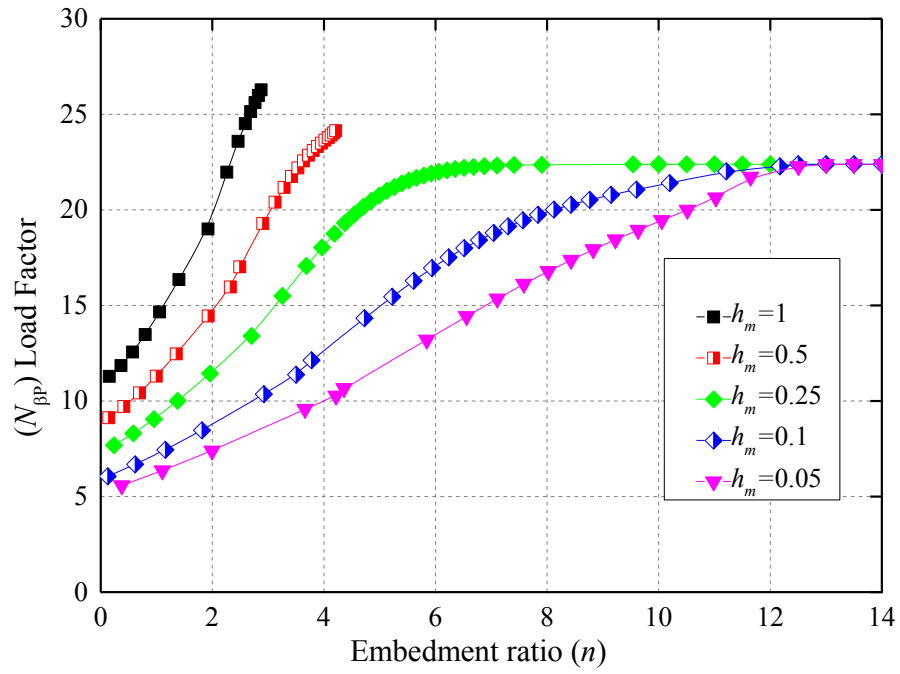


(a)  $\eta=0^\circ$

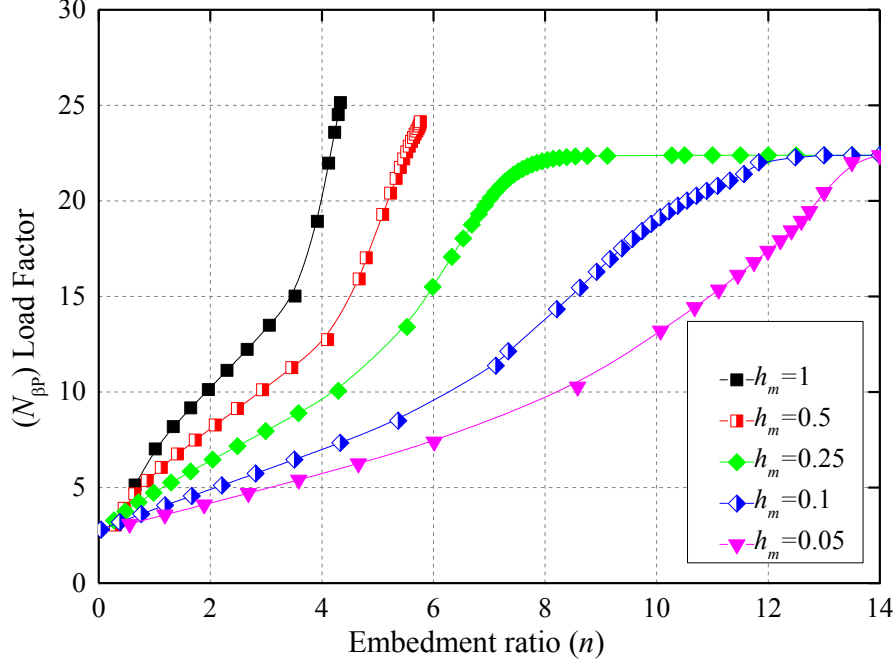




(b)  $\eta=20^\circ$



(c)  $\eta=40^\circ$

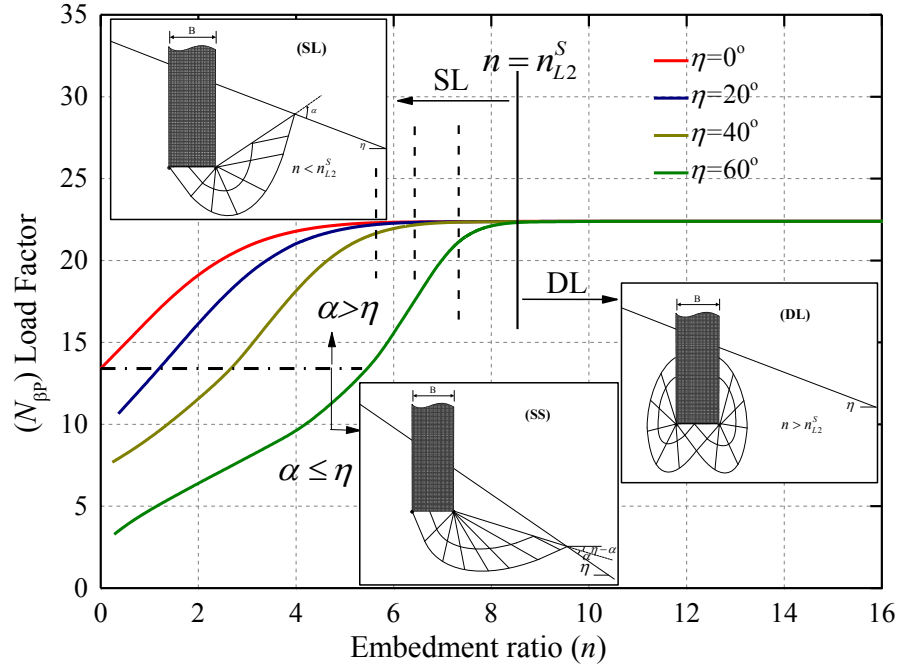


(d)  $\eta=60^\circ$

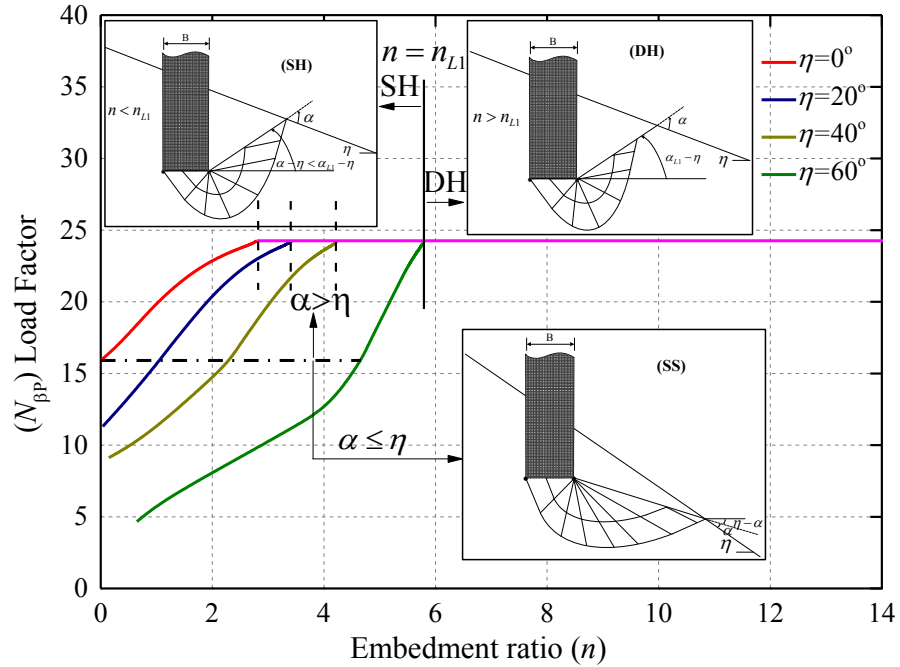
Fig.7. The relation between  $N_{\beta P}$  and  $n$  for different  $h_m$ .

Fig.8 shows the load factor  $N_{\beta P}$  against the embedment ratio  $n$  for different slope angles  $\eta$ . Fig.8 (a) shows that the load factor increases dramatically then tends to reach a constant value after  $n$  exceeds the limit embedment ratios  $n_{L2}^S$ , and the pile failure mode transits from SL to DL. Comparison between  $\eta=0^\circ \sim \eta=60^\circ$  reveals that the load factor will reach the constant value much later with increasing slope angles. That is to say, the limit embedment ratio  $n_{L2}^S$  increases with increasing slope angles. Fig.8 (b) shows that the load factor increases dramatically then end abruptly when intersected by the limit embedment ratio  $n_{L1}$  and the pile is under the failure mode of SH and will transit to DH failure mode as the embedment ratios increases further. Comparison between  $\eta=0^\circ \sim \eta=60^\circ$  reveals that the limit embedment ratio  $n_{L1}$  increases with increasing slope angles.

Additionally, whether  $h_m < 2\sqrt{2\zeta}$  or  $h_m > 2\sqrt{2\zeta}$ , if  $\alpha \leq \eta$ , the pile is under the failure mode of SS and will transit to SL or SH failure mode when  $\alpha > \eta$ .



(a)  $h_m < 2\sqrt{2\zeta}$  ( $h_m = 0.25$ )

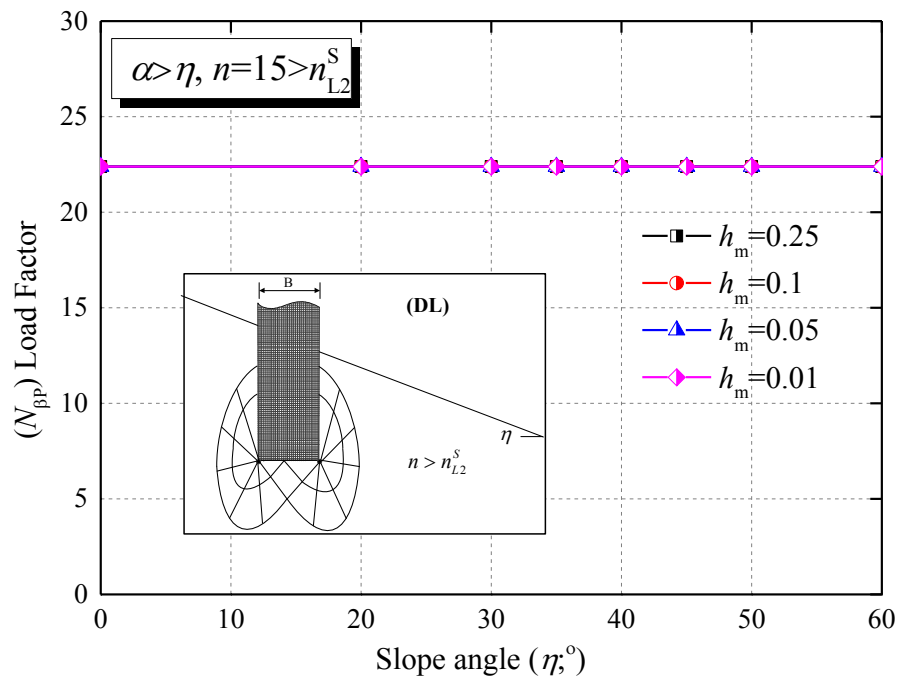


(b)  $h_m > 2\sqrt{2\zeta}$  ( $h_m = 0.5$ )

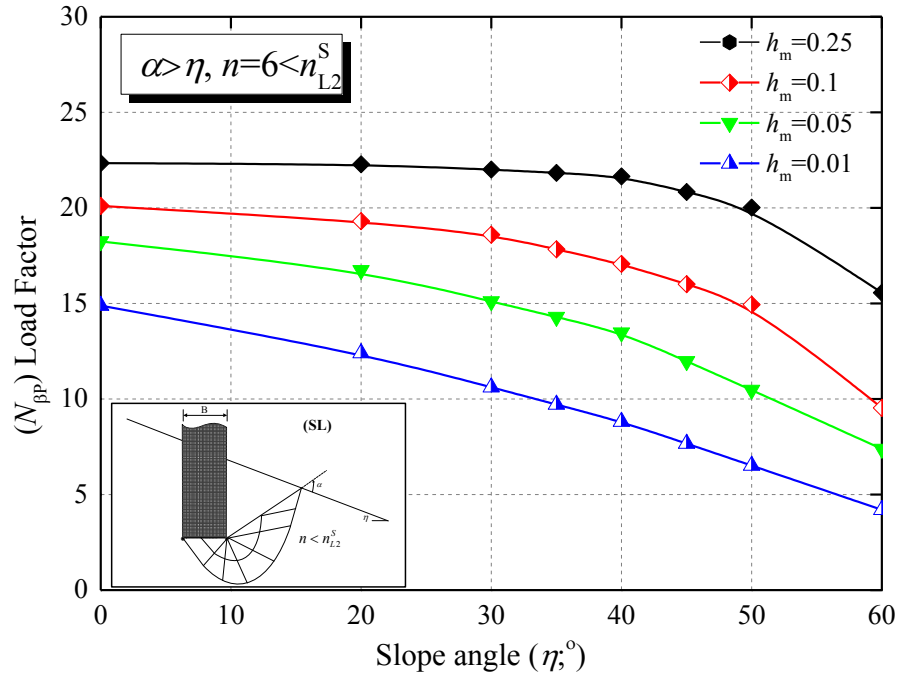
Fig.8. Variation in the load factor  $N_{\beta P}$  with embedment ratio  $n$  for different  $\eta$ .

Fig.9 shows the relation between the load factor  $N_{\beta P}$  and the slope angles  $\eta$  under five pile failure modes. Fig.9 (a) reveals that the load factors have no effects with increasing slope angles and the load factors are the same for different overburden pressures. Fig.9 (c) shows that the load factors also have no changes with increasing

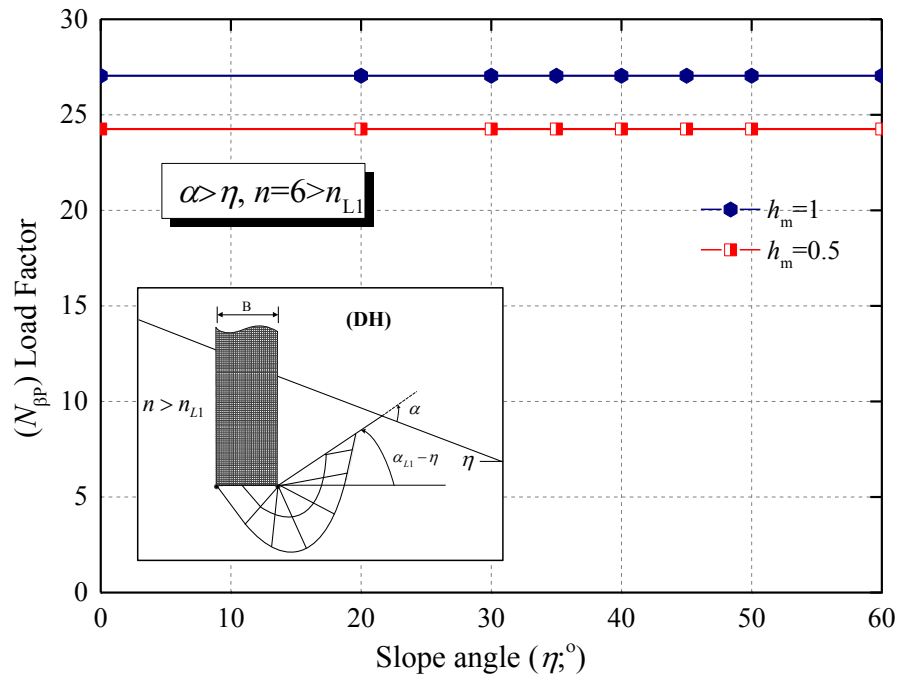
slope angles, but the overburden pressures have effects on the load factors. Fig.9 (b) shows that under the failure mode of SL, the load factors decrease with increasing slope angles for different overburden pressures  $h_m$ . When approximately  $\eta \leq 40^\circ$ , the load factors decrease moderately. When  $\eta > 40^\circ$ , the load factors decrease dramatically. For example, if  $h_m=0.25$ , the load factors decrease about 2.5% ( $\eta=0^\circ \sim 40^\circ$ ) and the load factors decrease about 35% ( $\eta=40^\circ \sim 60^\circ$ ). Fig.9 (d) reveals that the load factors also decrease with increasing slope angles, but  $\eta > 30^\circ$ , the load factors begin to decrease dramatically because of the effects of the overburden pressures. Fig.9 (e) shows that under the failure model of SS, the load factor has no demarcation point of overburden pressure load and the load factor decreases with increasing slope angles.



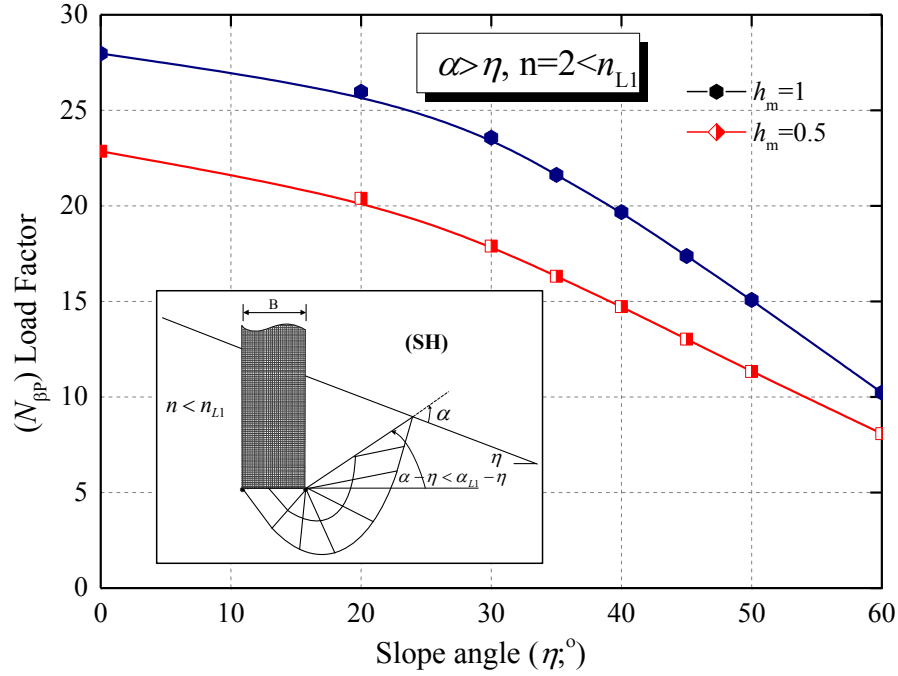
(a) Failure modes one (DL)



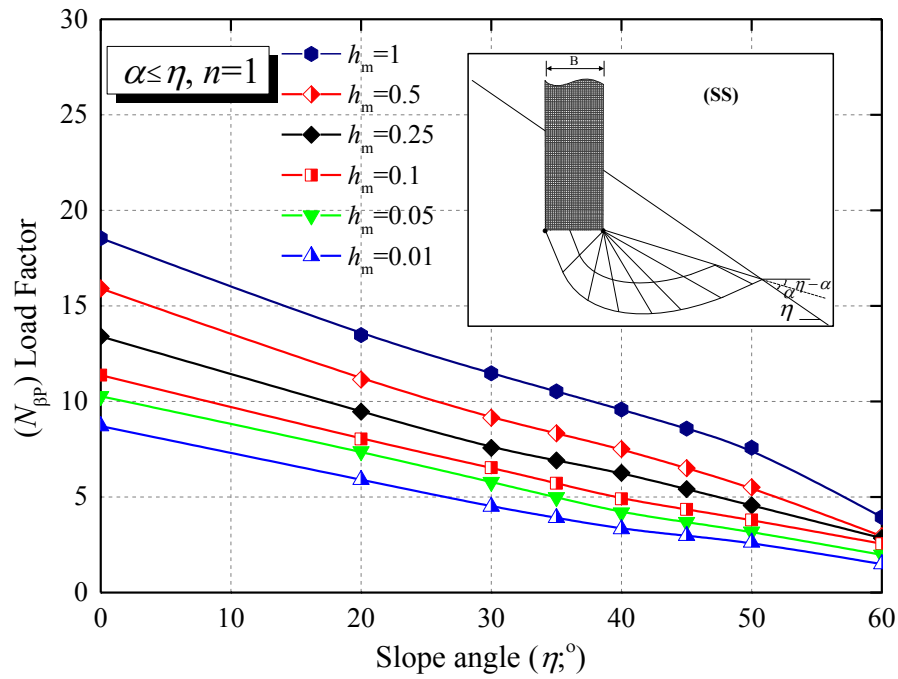
(b) Failure modes two (SL)



(c) Failure modes three (DH)



(d) Failure modes fore (SH)

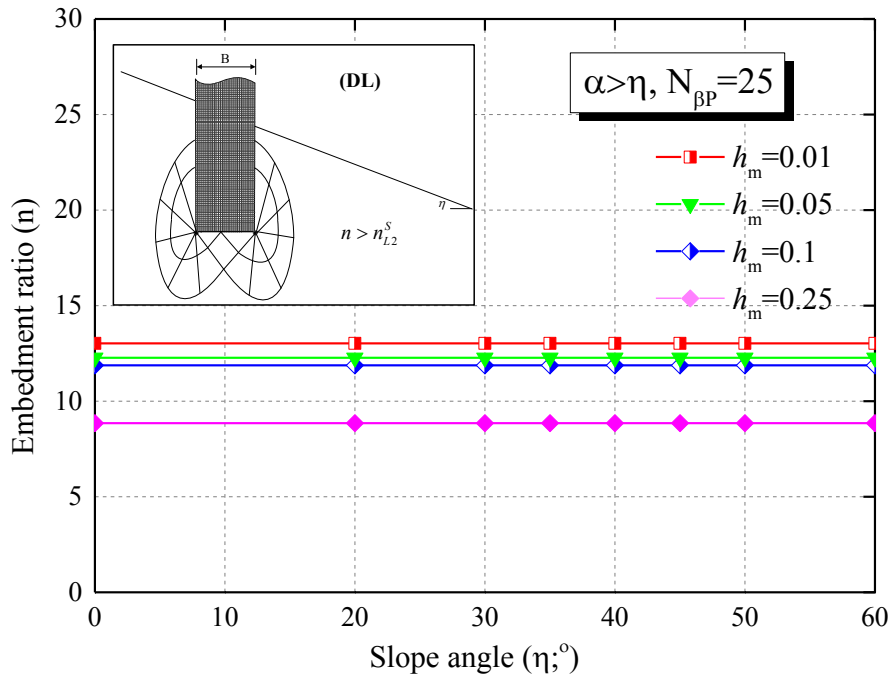


(e) Failure modes fore (SS)

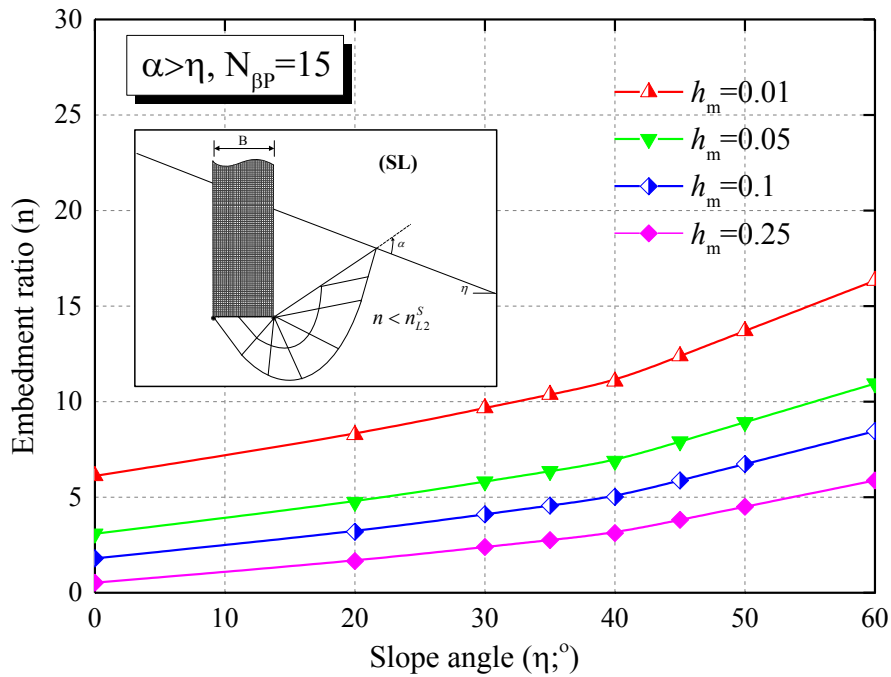
Fig.9 (a-e) Variation in the load factor  $N_{\beta P}$  with different values of  $\eta$ .

Fig.10 shows that the variation of the embedment ratio with the change of slope angles to get the same load factors  $N_{\beta P}$ . Fig.10 (a) and Fig.10 (c) reveal that the embedment ratios have no effects with increasing slope angles but the overburden pressures have effects on the embedment ratios. Fig.10 (b), Fig.10 (d) and Fig.10 (e) show that under the failure mode of SL, SH and SS, the load factors decrease with

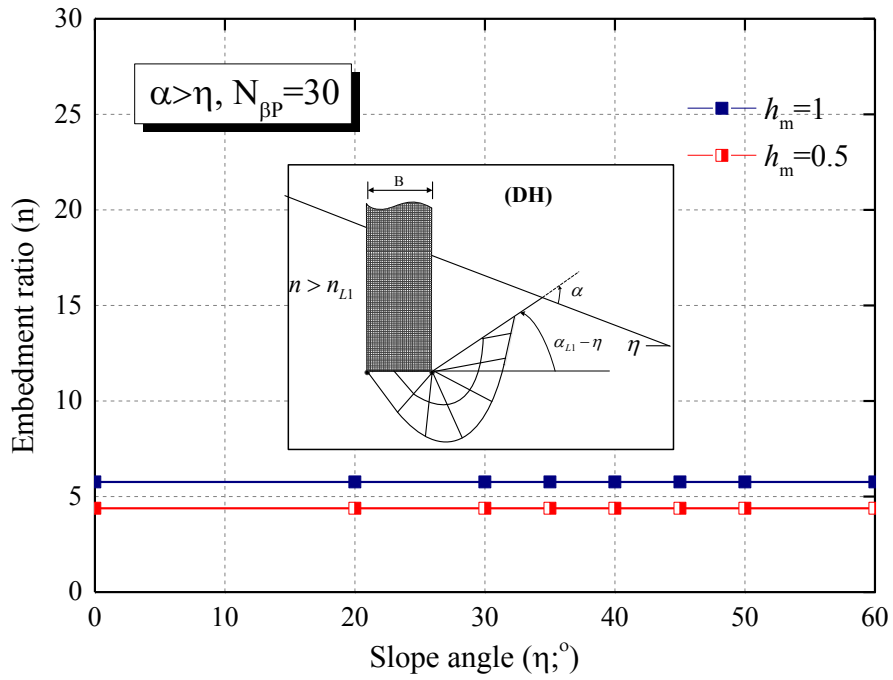
increasing slope angles for different overburden pressures  $h_m$ . When approximately  $\eta \leq 40^\circ$ , the embedment ratios increase moderately. When  $\eta > 40^\circ$ , the embedment ratios increase dramatically. For example, if the pile is under the mode of SL and  $h_m=0.01$ , the embedment ratios increase about 15% ( $\eta=0^\circ \sim 40^\circ$ ) and the embedment ratios increase about 25% ( $\eta=40^\circ \sim 60^\circ$ ).



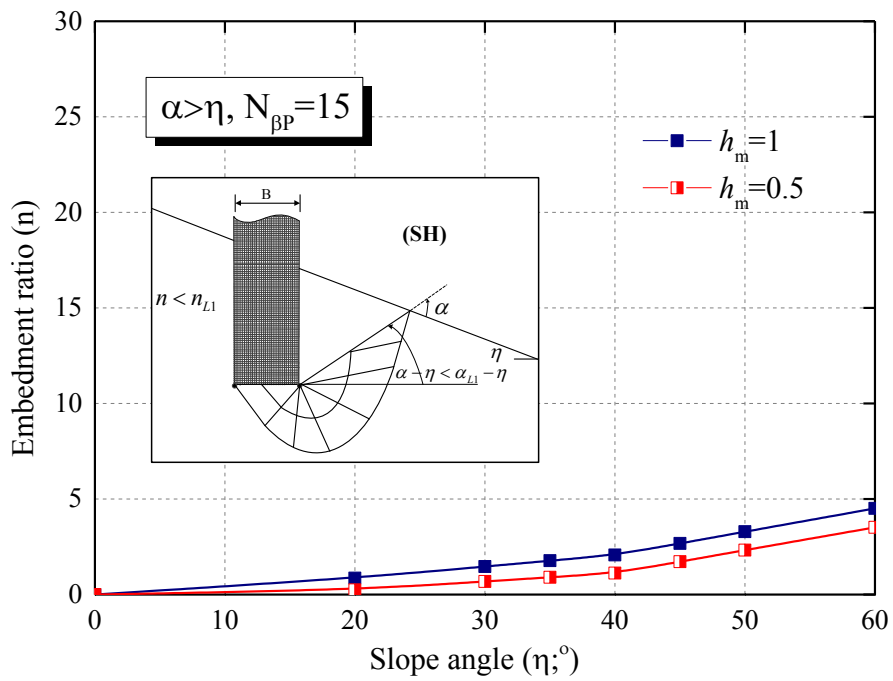
(a) Failure modes one (DL)



(b) Failure modes two (SL)

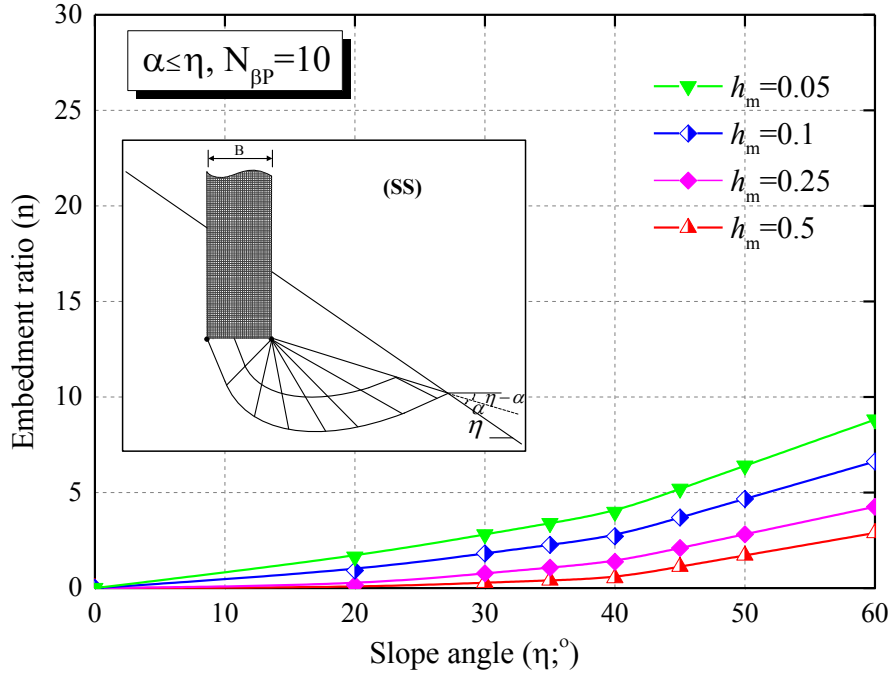


(c) Failure modes three (DH)



(d) Failure modes four (SH)





(e) Failure modes four (SS)

Fig. 10. (a-e) Variation in the embedment ratio  $n$  with different values of  $\eta$ , for different overburden pressures  $h_m$  ( $\zeta=0.01$ ).

The main limitation that emerges from the article is the non-consideration of the weight of rock mass, which limit the applicability of the study. All the theory of characteristic lines applied to foundations considers the analytical solution for a nearby slope of moderate inclination. This is because if the slope is strong, it becomes a problem of slope stability or global stability where the weight of the ground has a great relevance in the final solution. This aspect is crucial and must be clarified in which real configurations the study is valid because it is limited to some very specific cases and not as general as it is exposed in the article.

A comparison between the ultimate bearing capacity calculated by the finite element method and the value through the analytical solution was presented following. The ultimate bearing capacity at the tip of a pile is calculated using the following data:  $a=0.5$ ;  $\zeta=0.01$ ;  $\beta=1.932\text{Mpa}$ ;  $\gamma_R=30\text{KN/m}^3$ ;  $B=5\text{m}$ ;  $H_R=25\text{m}$ ;  $\gamma_S=18\text{KN/m}^3$ ;  $H_S=6\text{m}$ . Table.2 shows parameters of rocks for different slope angles.

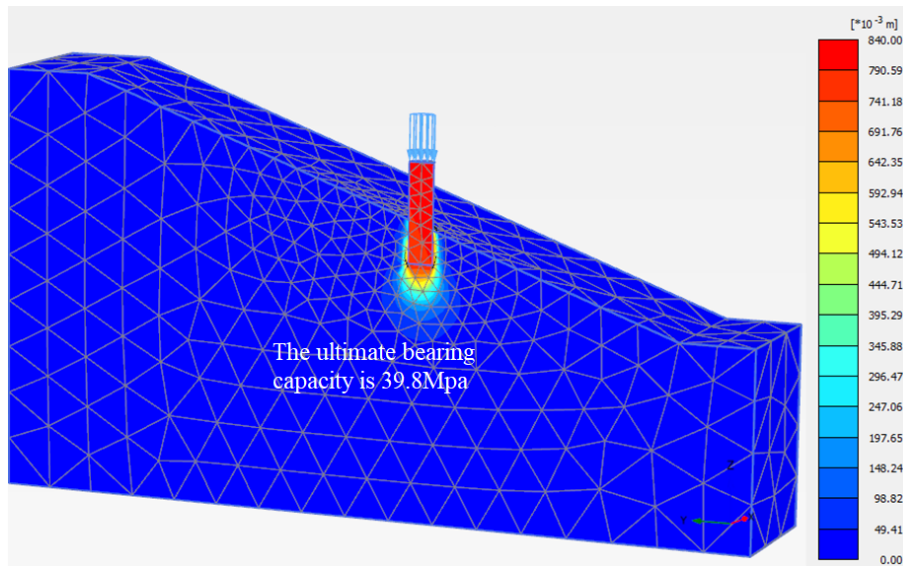
Table. 2 Parameter

Slope Angles $\eta$	Strength Modulus $\beta$	Tensile Strength $\zeta$	Virtual angles $\alpha$	Instantaneous angles $\rho_2$	Shape Coefficient $s_\beta$	Load Factor $N_{\beta P}$
20°	1.932 Mpa	0.01	83.79°	11.36°	1.33	21.9
40°	1.932 Mpa	0.01	89.78°	11.69°	1.31	20.75
60°	1.932 Mpa	0.01	47.32°	16.37	1.41	11.76

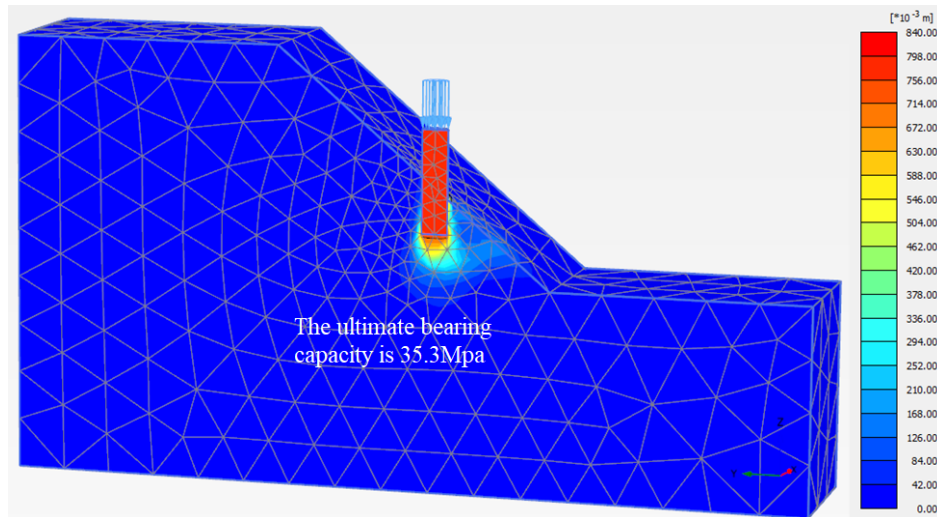
Through the analytical method, for  $\eta=20^\circ$ , the ultimate bearing capacity is  $\sigma_{hp}^* = \beta N_{\beta P} = 1.932 * 21.9 = 42.3 \text{Mpa}$ ; for  $\eta=40^\circ$ , the ultimate bearing capacity is  $\sigma_{hp}^* = \beta N_{\beta P} = 1.932 * 20.75 = 40.089 \text{Mpa}$ ; for  $\eta=60^\circ$ , the ultimate bearing capacity is  $\sigma_{hp}^* = \beta N_{\beta P} = 1.932 * 11.76 = 22.72 \text{Mpa}$ .

Fig.11 shows the finite element model to calculate ultimate bearing capacity at the tip of a pile for different slope angles. This model is established with the finite element software Plaxis 3D AE. The analysis method adopts the Hoek-Brown failure criterion.

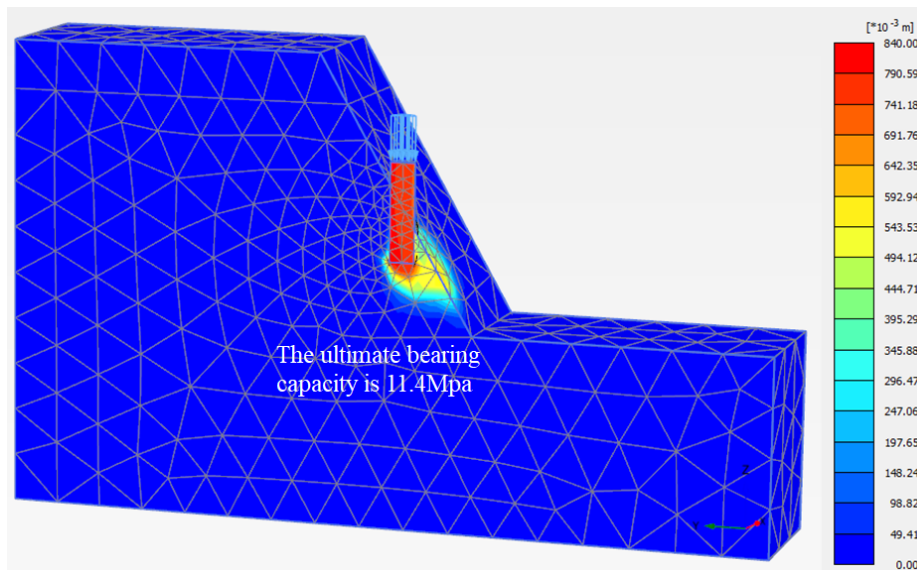
When  $\eta=20^\circ$ , the ultimate bearing capacity is 39.8Mpa. When  $\eta=40^\circ$ , the ultimate bearing capacity is 35.3Mpa. When  $\eta=60^\circ$ , the ultimate bearing capacity is 11.4Mpa.



(a)  $\eta=20^\circ$



(b)  $\eta=40^\circ$



(c)  $\eta=60^\circ$

Fig.11. (a-c) Finite element method to calculate ultimate bearing capacity at the tip of a pile for different slope angles.

The weight of rock mass was not considered in the analytical method, which may exert an impact on the ultimate bearing capacity at the tip of a pile. For a certain range of slope angles, the impact is relatively small. In this case (see Fig.12),  $\eta=40^\circ$  is approximately the turning point. When  $\eta < 40^\circ$ , the difference of the bearing capacity between the analytical method and the finite element method is small, thus the analytical method is applicable at this range of slope angles. When  $\eta > 40^\circ$ , the gap between the analytical results and numerical results is enlarged and the errors

caused by the neglect of weight of rock mass in the analytical method becomes unacceptable.

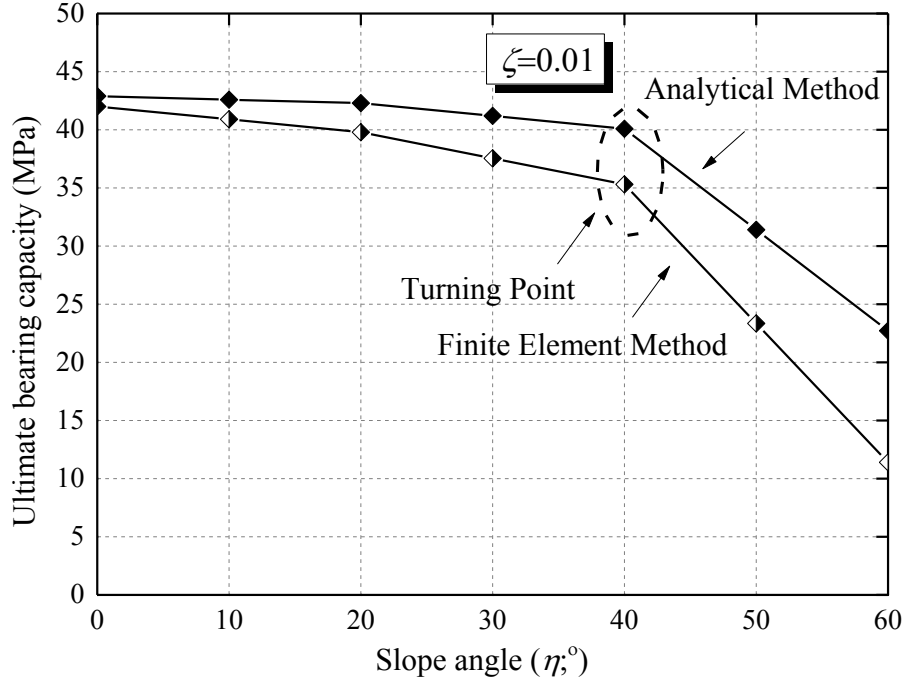


Fig.12. The relation between the ultimate bearing capacity and different slope angles.

## 5. Summary and conclusions

An analytical method for calculating the ultimate bearing capacity of inclined rock piles with different slope angles is proposed based on the characteristic line method. Different failure modes of piles were determined under different embedment ratios and slope angles. The influence of slope angle and the pile embedment ratio on the pile bearing capacity was analyzed. The main conclusions can be drawn as following:

1. For the case of the virtual angle  $\alpha$  is larger than the slope angle  $\eta$ , four different failure modes exist for piles in the inclined rock. When  $h_m < 2\sqrt{2\zeta}$ , the failure mode of the pile were divided by the limiting embedment ratio  $n_{L2}^S$  into DL ( $n > n_{L2}^S$ ) and SL ( $n < n_{L2}^S$ ), and the limiting embedment ratio  $n_{L2}^S$  increases with increasing slope angles. When  $h_m > 2\sqrt{2\zeta}$ , the failure mode of the pile were divided by the limiting embedment ratio  $n_{L1}$  into DH ( $n > n_{L1}$ ) and SH ( $n < n_{L1}$ ), and the limiting embedment ratio  $n_{L1}$  increases with increasing slope angles  $\eta$ , especially when

$\eta > 40^\circ$ .

2. For the case of the virtual angle  $\alpha$  is smaller than the slope angle  $\eta$ , one pile failure mode, shallow foundation piles (SS), can occur.
3. Under the pile failure mode of DL and the mode of DH, the ultimate bearing capacity at the tip of a pile has no change with the variation of slope angles. In addition under the failure mode of DH, the ultimate bearing capacity increases with the overburden pressures.
4. Under the modes of SL, SH and SS, the ultimate bearing capacity at the tip of a pile decreases with increasing rate as the slope angle increases. To get the same ultimate bearing capacity at the pile tip, the pile embedment ratio should increase. The proposed analytical method can be served as an efficient method to estimate the bearing capacity of piles in inclined slope with small slope angle (typically less than  $40^\circ$ ).

### **Acknowledgements**

The authors are grateful to the support of National Key R&D Program of China (2016YFC0800200) , and the National Natural Science Foundation of China (Grant Nos. 51778571, 51578500, 51578426). This paper has also received funding from the European Union's Horizon 2020 MARIE SKLODOWSKA-CURIE RESEARCH AND INNOVATION STAFF EXCHANGE Program under the grant No 778360.

### **References**

- [1] Terzaghi K, Terzaghi K P R B, Terzaghi K P R B. Theoretical soil mechanics[J]. John Wiley & Sons, 1965.
- [2] Verdu S, Han T S. A general formula for channel capacity [J]. Information Theory IEEE Transactions on, 2008, 40(4):1147-1157.
- [3] Meyerhof, G. G. The Ultimate Bearing Capacity of Foudations [J]. Géotechnique, 1951, 2(4):301-332.
- [4] Sokolovsky V.V Statics of Loose medium [M]. 1956.
- [5] Serrano A, Olalla C. Ultimate bearing capacity of an anisotropic rock mass, part I: basic modes of failure. International Journal of Rock Mechanics & Mining Sciences, 1998;35(3):301 - 24.
- [6] Serrano A, Olalla C. Ultimate bearing capacity of an anisotropic rock mass, part II: procedure for its determination. International Journal of Rock Mechanics & Mining

Sciences, 1998;35(3):325 – 48.

[7] Serrano A, Olalla C. Ultimate bearing capacity of rock masses. *International Journal of Rock Mechanics & Mining Sciences*, 1994;31:93 – 106.

[8] Serrano A, Olalla C. Ultimate bearing capacity of an anisotropic discontinuous rock mass. Part I: Basic modes of failure [J]. *International Journal of Rock Mechanics & Mining Sciences*, 1998, 35(3):301-324.

[9] Serrano A , Olalla C, J González. Ultimate bearing capacity of rock masses based on the modified Hoek – Brown criterion [J]. *International Journal of Rock Mechanics & Mining Sciences*, 2000, 37(6):1013-1018.

[10] Yang X L , Yin J H . Upper bound solution for ultimate bearing capacity with a modified Hoek-Brown failure criterion [J]. *International Journal of Rock Mechanics & Mining Sciences*, 2005, 42(4):550-560.

[11] Yang X L, Yin J H. Linear Mohr – Coulomb strength parameters from the non-linear Hoek-Brown rock masses [J]. *International Journal of Non-Linear Mechanics*, 2006, 41(8):1000-1005.

[12] Galindo R A, Serrano A, Olalla C. Ultimate bearing capacity of rock masses based on modified Mohr-Coulomb strength criterion [J]. *International Journal of Rock Mechanics and Mining Sciences*, 2017, 93:215-225.

[13] Serrano A, Olalla C, J González. Ultimate bearing capacity of rock masses based on the modified Hoek-Brown criterion [J]. *International Journal of Rock Mechanics & Mining Sciences*, 2000, 37(6):1013-1018.

[14] Cheng Y M, Au S K. Solution of the bearing capacity problem by the slip line method [J]. *Canadian Geotechnical Journal*, 2005, 42(4):1232-1241.

[15] Cheng Y M, Li D Z, Li L, et al. Limit equilibrium method based on an approximate lower bound method with a variable factor of safety that can consider residual strength[J]. *Computers & Geotechnics*, 2011, 38(5):623-637.

[16] Serrano A, Olalla C. Ultimate bearing capacity at the tip of a pile in rock - Part 1: Theory [J]. *International Journal of Rock Mechanics & Mining Sciences*, 2002, 39(7):833-846.

[17] Serrano A, Olalla C. Ultimate bearing capacity at the tip of a pile in rock—part 2: application [J]. *International Journal of Rock Mechanics and Mining Sciences*, 2002, 39(7):847-866.

[18] Hoek E, Brown ET. Empirical strength criterion for rock masses. *Journal of the*

Fig.1. Sketch of assumed failure

Fig.2. Force diagram and stress ellipses.

Fig.3. The relation between the embedment ratio  $n$  and the overburden pressure  $h_m$  for different  $\zeta$ .

Fig.4. Failures modes of pile under the different slope angles  $\eta$  ( $\alpha > \eta$ ).

Fig.5. The variation of the limiting embedment ratio with the change of slope angles.

Fig.6. Failures modes of pile under the different slope angles  $\eta$  ( $\alpha \leq \eta$ ).

Fig.7. The relation between  $N_{\beta P}$  and  $n$  for different  $h_m$ .

Fig.8. Variation in the load factor  $N_{\beta P}$  with embedment ratio  $n$  for different  $\eta$ .

Fig.9 (a-e) Variation in the load factor  $N_{\beta P}$  with different values of  $\eta$ .

Fig.10. (a-e) Variation in the embedment ratio  $n$  with different values of  $\eta$ , for different overburden pressures  $h_m$  ( $\zeta=0.01$ ).

Fig.11. (a-c) Finite element method to calculate ultimate bearing capacity at the tip of a pile for different slope angles.

Fig.12. The relation between the ultimate bearing capacity and different slope angles.

Table. 1 Failure modes of piles in inclined rock

Table. 2 Parameter

